Analytica Chimica Acta 1103 (2020) 156–163

Contents lists available at ScienceDirect

Analytica Chimica Acta

journal homepage: www.elsevier.com/locate/aca

Responsive nanosensor for ratiometric luminescence detection of hydrogen sulfide in inflammatory cancer cells

Jianping Liu [a, 1], Chengchen Duan [a, 1], Wenzhu Zhang [b], Hang Thu Ta [a, c], Jingli Yuan [b], Run Zhang [a, *], Zhi Ping Xu [a, **]

[a] Australian Institute for Bioengineering and Nanotechnology (AIBN), The University of Queensland, Brisbane, 4072, Australia
[b] State Key Laboratory of Fine Chemicals, School of Chemistry, Dalian University of Technology, Dalian, 116024, China
[c] School of Pharmacy, University of Queensland, Woollongabba, QLD, 4102, Australia

HIGHLIGHTS

- A mesoporous silica nanoparticle-based responsive nanosensor is developed for hydrogen sulphide (H_2S) detection.
- The new nanosensor can rapidly and selectively respond to H_2S and give ratiometric luminescence signal changes.
- Nanosensor can be internalized to cells through plasma membrane receptors and/or microtubules-mediated endocytosis.
- The application of nanosensor for the detection of H_2S level changes in live cancer cells is demonstrated.

GRAPHICAL ABSTRACT

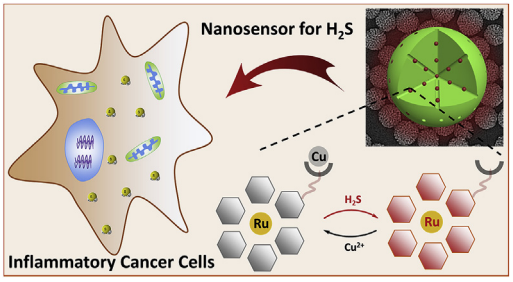

ARTICLE INFO

Article history:
Received 1 October 2019
Received in revised form
10 December 2019
Accepted 19 December 2019
Available online 20 December 2019

Keywords:
Responsive nanosensor
Ratiometric luminescence
Hydrogen sulfide detection
Mesoporous silica nanoparticle
Inflammatory cancer cells

ABSTRACT

Gasotransmitter hydrogen sulfide (H_2S), produced enzymatically in body, has important functions in biological signaling and metabolic processes. An abnormal level of H_2S expression is associated with different diseases, therefore, development of novel bioanalytical methods for rapid and effective detection of H_2S in biological conditions is of great importance. In this work, we report the development of a new responsive nanosensor for ratiometric luminescence detection of H_2S in aqueous solution and live cells. The nanosensor (**Ru@FITC-MSN**) was prepared by immobilizing a luminescent ruthenium(II) (Ru(II)) complex into a fluorescein isothiocyanate (FITC) conjugated water-dispersible mesoporous silica nanoparticle (MSN), showing dual emission bands at 520 nm (FITC) and 600 nm (Ru complex). The red luminescence of the formed **Ru@FITC-MSN** was quenched in the presence of Cu^{2+}. The in-situ generated **Ru**–**Cu@FITC-MSN** responded to H_2S rapidly and selectively, showing a linear ratiometric luminescence change in FITC and Ru(II) channels with the H_2S concentration (0.5–4 μM). Limit of detection (LoD) and limit of quantification (LoQ) were determined to be 0.36 and 1.21 μM. Followed by investigation of cellular uptake processes, the utility of the nanosensor for ratiometric imaging of H_2S in live cells and its capability to monitor H_2S levels in inflammatory breast cancer cells were then demonstrated. This study provides a powerful approach for detection of highly reactive and unstable H_2S biomolecules in live systems.

* Corresponding author.
** Corresponding author.
E-mail addresses: r.zhang@uq.edu.au (R. Zhang), gordonxu@uq.edu.au (Z.P. Xu).
[1] These authors contributed equally to this work.

https://doi.org/10.1016/j.aca.2019.12.056
0003-2670/

1. Introduction

Advanced early disease diagnosis and treatment monitoring necessitate the development of new bioanalytical methods for detection of unstable and highly reactive biomarkers [1,2]. These biomarkers normally include reactive oxygen/nitrogen/carbon species (ROS/RNS/RCS) and gasotransmitters, such as hydrogen sulfide (H_2S), nitric oxide (NO), sulfide dioxide (SO_2) and carbon monoxide (CO) [3–5]. Compared to ROS/RNS/RCS, gasotransmitters, especially H_2S, are less investigated as they have been granted as the toxic gases for biological and environmental systems for many years [6–8]. Recent research data have revealed that H_2S is endogenously generated by three principal enzymes: cystathionine-β-synthase (CBS), cystathionine-γ-lyase (CSE), and 3-mercaptopyruvate sulfurtransferase (MST) [3]. Similar to NO, this gaseous molecule contributes significantly to various biological processes, such as neurotransmission, vasorelaxation, and anti-inflammation [3]. The H_2S level changes in body are associated with several diseases, such as Alzheimer's disease, Down's syndrome, diabetes, liver cirrhosis, and even cancers [8]. In particularly, the H_2S level is directly implicated with the inflammation of the cancer cells, but its simple and quick determination is scarcely reported [3].

Reliable bioanalytical methods for highly specific and sensitive detection of H_2S is key for investigation of H_2S functions in biological systems [6]. Over the past few decades, several techniques have been reported for H_2S detection in bulk solution [9–14]. Of various approaches, optical detection using H_2S responsive sensors has been recognized as one of the most promising technology due to its inherent advantages, such as high sensitivity and simplicity, rapidity, and efficiency [15,16]. The H_2S responsive sensors are normally designed based on different sensing mechanisms, such as thiolysis of dinitrophenyl ether [17–21], reaction with azide [22–31], nucleophilic addition with formaldehyde groups [32,33], and displacement of metal ions from luminescent dyes [34–38]. By virtue of these reactions, several sensors have been developed for sensitive and selective H_2S detection and H_2S visualization in live cells and organisms (Table S1) [26,39–42]. The majority of the reported H_2S sensors are designed based on the "OFF-ON" changes of luminescent signals [6,43]. The luminescence signal is easily interfered with the autofluorescence signal from biomolecules, giving false-positive/negative detection. Ratiometric luminescent sensors are desirable because the self-referenced changes of the luminescent signals are more reliable for H_2S detection in biological systems [2,44].

In this contribution, we report the design and synthesis of a new responsive luminescence nanosensor for ratiometric detection of H_2S and evaluate its application in detecting H_2S in inflammatory cancer cells. As shown in Scheme 1, the mesoporous silica nanoparticle (MSN)-based sensor consists a conjugated fluorescein isothiocyanate (FITC) as the reference signal and an embedded ruthenium(II) (Ru(II)) complex as the H_2S responsive unit. The prepared **Ru@FITC-MSN** nanoparticles emit two luminescence emission bands cantered at 520 nm (FITC) and 600 nm (Ru(II) complex). The emission of Ru(II) complex is quenched upon addition of copper ion (Cu^{2+}) [45], and the in-situ formed **Ru–Cu@FITC-MSN** nanosensor turn on the emission of Ru(II) complex upon the specific reaction with H_2S in HEPES buffer solution, showing the ratiometric luminescence response to H_2S in solution. The nanosensor is featured with high selectivity, sensitivity and fast response to H_2S detection, and good biocompatibility, as demonstrated in this research. The cellular internalization processes were optimized and the uptake mechanism investigated, followed by imaging of H_2S in live breast cancer cells. Moreover, flow cytometry analysis of endogenous H_2S level changes in inflammatory MCF-7 cells was demonstrated, providing direct evidence about the H_2S formation in inflammatory cancer cells.

2. Experimental section

2.1. Materials and physicochemical characterization

Ruthenium complex, $[Ru(bpy)_2(bpy\text{-}DPA)]^{2+}$, was prepared and characterized following previously reported method [46]. Fluorescein isothiocyanate (FITC), (3-aminopropyl)triethoxysilane (APTES), tetraethyl orthosilicate (TEOS), 3-(4,5-dimethylthiazol-2-yl)-2,5-diphenyltetrazolium bromide (MTT), lipopolysaccharide (LPS), chloroquine, filipin, nocodazole, colchicine, ammonium chloride, and dexamethasone were purchased from Sigma-Aldrich. Dulbecco's Modified Eagle's Medium (DMEM), fetal bovine serum (FBS), L-glutamine, penicillin, and streptomycin sulfate were purchased from Life Technologies. Unless otherwise stated, all chemical materials were purchased from commercial sources and used without further purification. All water used in experiments was double distilled and filtered with Elga Purelab® Ultrapure Water purification system.

The morphology and size of nanoparticles were characterized using transmission electron microscope (TEM) (Hitachi HT 7700) operated at an acceleration voltage of 120 kV. The samples for TEM images were dispersed in water and then dropped on a copper grid. Small angle X-ray powder diffraction (SAXRD) patterns were collected on a PAN alytical X'Pert Pro MPD X-ray diffractometer using Cu $K\alpha 1$ radiation (40 kV, 40 mA, $\lambda = 0.15418$ nm). The nanoparticle zeta potential in aqueous suspension was measured on a Nano Zeta-Sizer (Malvern instruments). Nitrogen adsorption-desorption isotherms were measured using a TriStar II Surface Area and Porosity analyser (Micromeritics). Fourier transform infrared (FTIR) spectra were collected on a Nicolet iS10 spectrometer (Thermo Fisher Scientific Inc., USA) at a resolution of 4 cm^{-1} for 32 scans. Thermogravimetric analysis (TGA) was conducted on a Mettler Toledo TGA LF1600. UV–Vis spectra were recorded on UV-2401 PC spectrometer (Shimazu). Luminescence spectra were measured on FR-5310 PC (Shimadzu) and FS 920 (Edinburgh) spectrometers. Confocal luminescence imaging experiments were carried out on a Leica SP8 laser-scanning microscope. The image analysis was performed by ImageJ software version 1.44p. Flow cytometry analysis was performed on an Accuri C6 flow cytometer with a 488 nm laser excitation and an emission filter of 585/40 nm. The data were analyzed with CytExpert software.

2.2. Preparation of FITC-doped mesoporous silica nanoparticles (FITC-MSN)

Following literature report [47], FITC-APTES precursor was first synthesized by stirring of FITC (18.7 mg) and APTES (41.58 μL) in dimethylformamide (DMF) at room temperature in a dark room for 2 h. The stock solution of FITC-APTES was sealed and kept in dark for further use.

To prepare FITC-MSN, triethanolamine (TEA, 0.1 mL) in 30 mL water solution was heated to 95 °C. Cetyltrimethylammonium chloride (CTAC, 25 wt%, 6.45 mL) was then added and the mixture was stirred at 95 °C for 10 min before slowly addition of TEOS (0.5 mL) and FITC-APTES (50 μL) stock solutions. Ethyl acetate (0.5 mL) was then added into the solution, and the mixture was further stirred at 95 °C for 1 h. After cooling down to room temperature, the formed nanoparticles were collected by centrifugation (20,000 rpm) for 10 min. The nanoparticles were washed with 98% ethanol (20 mL) for three times. The FITC-MSN was then obtained by washing as-prepared nanoparticles with NaCl saturated methanol solution, and then freeze-dried for further

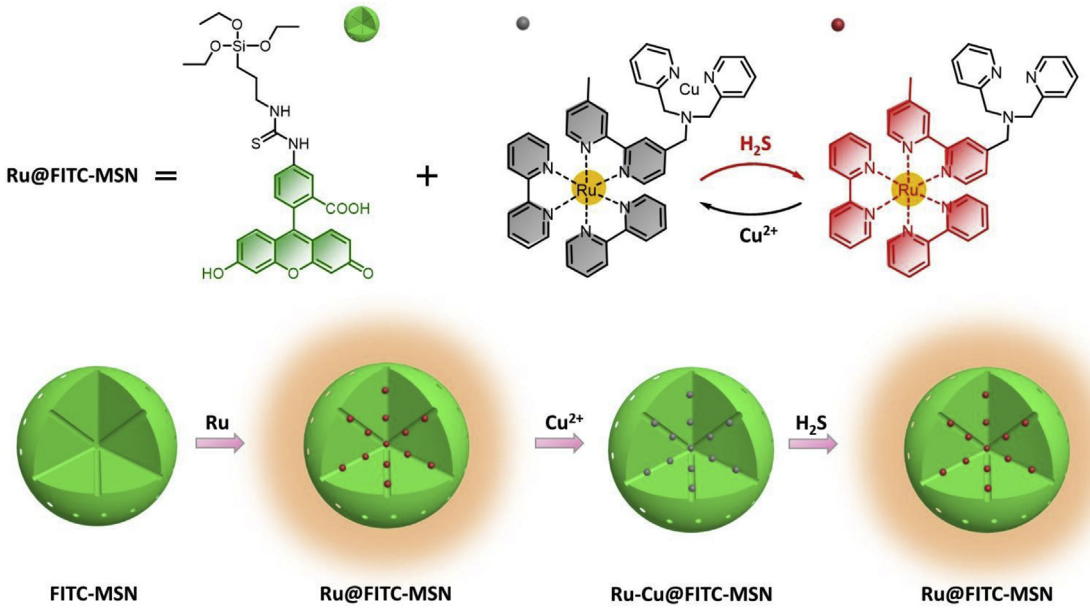

Scheme 1. Schematic illustration the strategy and the preparation of responsive nanosensor for H_2S detection.

characterization and ruthenium(II) complex loading.

2.3. Preparation of Ru@FITC-MSN and Ru–Cu@FITC-MSN

As-prepared FITC-MSN (11 mg) was added into $[Ru(bpy)_2(bpy\text{-}DPA)]^{2+}$ (9.76 mg) in DMF [46] and the mixture was stirred at room temperature for 48 h. The formed **Ru@FITC-MSN** was collected by centrifugation at 20,000 rpm for 10 min, and then washed with water for three times to remove excess $[Ru(bpy)_2(bpy\text{-}DPA)]^{2+}$. The **Ru–Cu@FITC-MSN** was prepared in-situ by addition of Cu^{2+} to **Ru@FITC-MSN** in aqueous solution. The **Ru–Cu@FITC-MSN** was then collected by centrifugation at 20,000 rpm for 10 min and washed with water for three times. The prepared **Ru@FITC-MSN** and **Ru–Cu@FITC-MSN** were freeze-dried for further use.

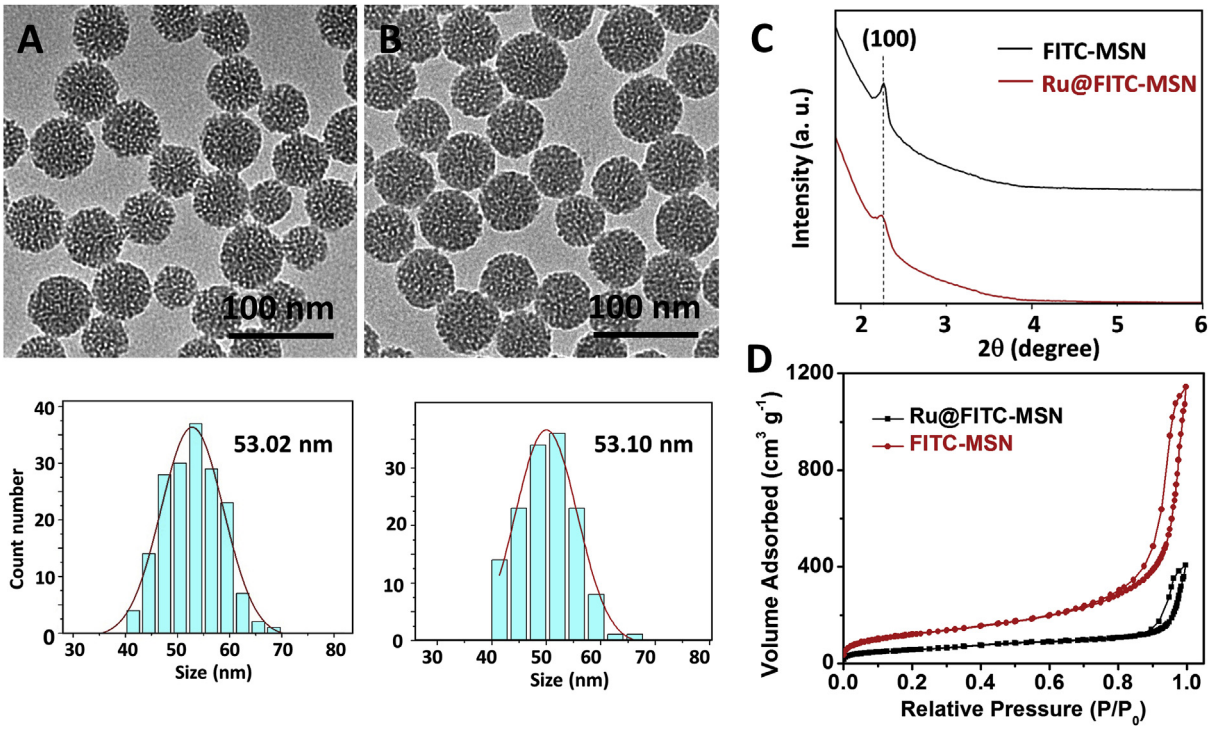

Fig. 1. Characterization of prepared nanosensor. TEM images and size distribution of FITC-MSN (A) and **Ru@FITC-MSN** (B). XRD pattern (C) and Nitrogen adsorption/desorption isotherms (D) of FITC-MSN and **Ru@FITC-MSN**.

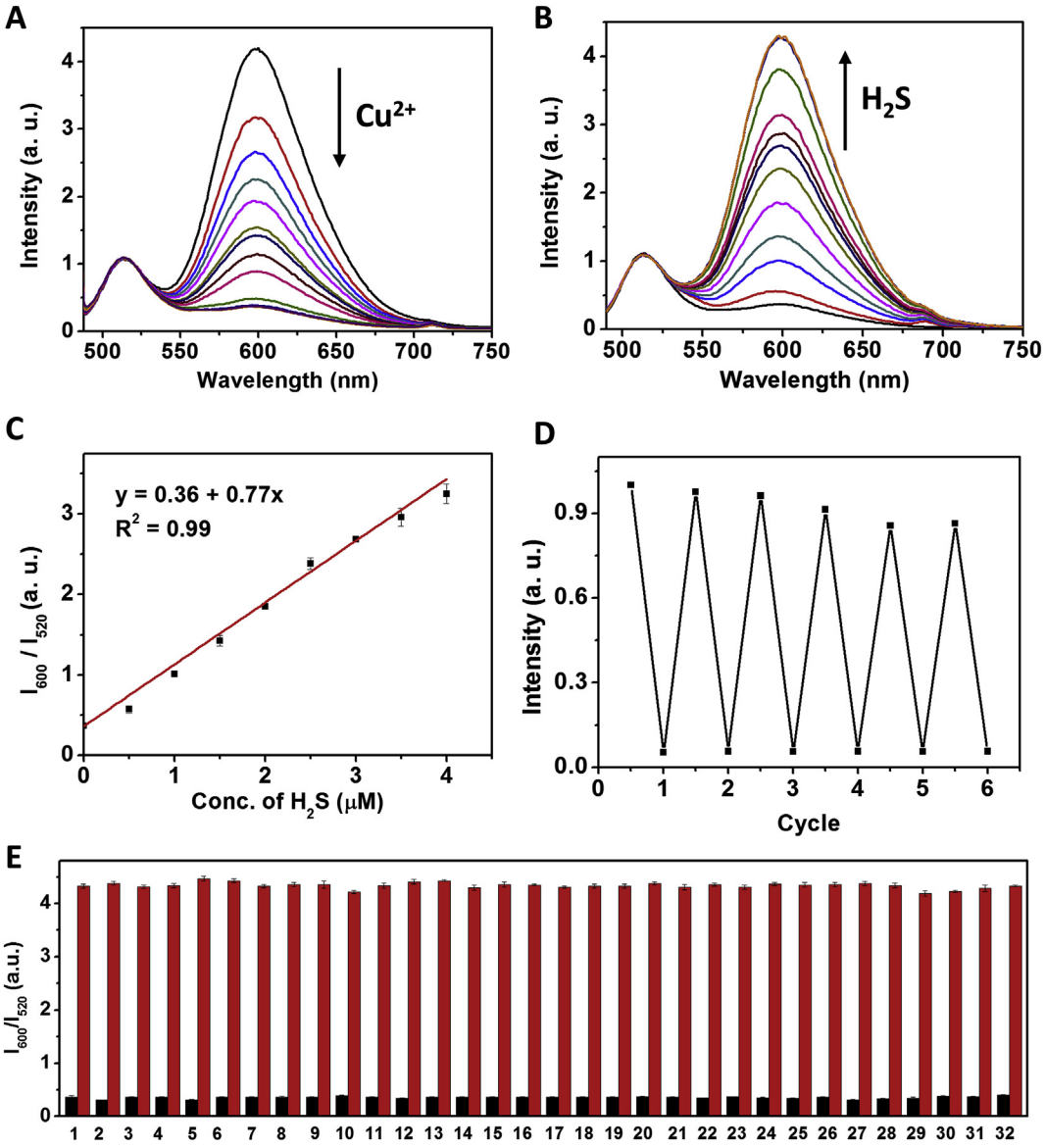

Fig. 2. Ratiometric luminescence response of in-situ generated **Ru**–**Cu@FITC-MSN** to H_2S. (A) Emission spectra of **Ru@FITC-MSN** in the presence of Cu^{2+} at different concentrations: 0, 0.2, 0.4, 0.8, 1, 1.5, 2, 4, 6, 8, 10 μM. (B) Emission spectra of **Ru**–**Cu@FITC-MSN** in the presence of H_2S at different concentrations: 0, 0.2, 0.4, 0.8, 1, 1.5, 2, 4, 6, 8, 10 μM. (C) Standard curve for H_2S detection. (D) The recyclability of Ru–Cu@FITC-MSN nanosensor for H_2S detection. **Ru**–**Cu@FITC-MSN** was added with 6 μM Cu^{2+}, and then added with 6 μM NaHS. The cycles were repeated six times. (E) Changes of **Ru**–**Cu@FITC-MSN** emission (I_{600}/I_{520}) in the presence of different anions (50 μM), reactive oxygen species (ROS, 50 μM) and biomolecules (1 mM). The competitive species include: (1) blank, (2) NO_3^-, (3) NO_2^-, (4) F^-, (5) I^-, (6) Cl^-, (7) $S_2O_8^{2-}$, (8) SO_4^{2-}, (9) $S_2O_5^{2-}$, (10) $S_2O_3^{2-}$, (11) $P_2O_7^{4-}$, (12) $P_3O_{10}^{5-}$, (13) $H_2PO_4^-$, (14) HPO_4^{2-}, (15) CO_3^{2-}, (16) HCO_3^-, (17) AcO^-, (18) MoO_4^{2-}, (19) $B_4O_7^{2-}$, (20) N_3^-, (21) HOCl, (22) NO, (23) •OH, (24) H_2O_2, (25) Cys, (26) Hcy, (27) GSH, (28) Br^-, (29) PO_4^{3-}, (30) SO_3^{2-}, (31) SCN^-, and (32) the mixture. Data were collected at room temperature in HEPES buffer of pH 7.4. The excitation wavelength was 450 nm.

3. Results and discussion

3.1. Physicochemical features of nanosensor

The FITC conjugated silica precursor, FITC-APTES, was first prepared by reacting of isothiocyanate with amino group of (3-aminopropyl)triethoxysilane (APTES) according to the method [47]. Co-condensation of FITC-APTES and TEOS in the presence of CTAC readily doped silica nanoparticles with FITC. Then, the FITC-MSN was formed by further washing with NaCl saturated methanol solution following a published procedure to remove CTAC [48]. As shown in Fig. S1, the FTIR spectrum of FITC-MSN shows that the surfactant CTAC was completely removed due to the absence of the characteristic peak of C–N stretching in 3000-2800 cm^{-1} [49]. The prepared FITC-MSN was well dispersed in water with the averaged size of 53 nm (Fig. 1A). The spherical morphology of the FITC-MSN showed ζ-potential of −11.4 mV in pure water. The amount of FITC doped was around 14 wt% by thermogravimetric analysis (TGA) under nitrogen atmosphere (Fig. S2). As shown in Fig. 1C, the small-angle X-ray diffraction (SAXRD) pattern of FITC-MSN displays a typical hexagonally packed mesoporous structure. Moreover, the nitrogen adsorption-desorption isotherm analysis suggests that the FITC-MSN had a pore volume of 0.52 $cm^3\ g^{-1}$ and surface area of 130.2 $m^2\ g^{-1}$ (Fig. 1D).

The **Ru@FITC-MSN** was then prepared by loading $[Ru(bpy)_2(bpy\text{-}DPA)]^{2+}$ into the mesoporous of FITC-MSN, followed by washing to remove free Ru(II) complexes. The encapsulating of $[Ru(bpy)_2(bpy\text{-}DPA)]^{2+}$ to the FITC-MSN is attributed to the

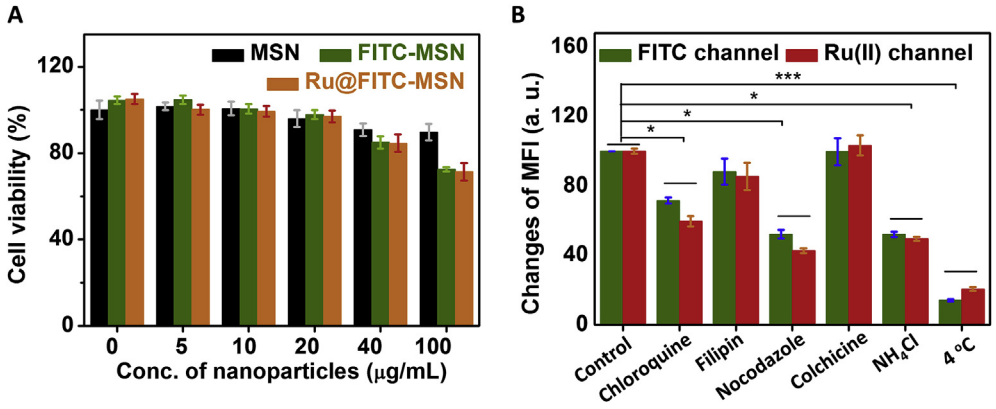

Fig. 3. Evaluation of cytotoxicity (A) and cellular internalization mechanism (B) of nanoparticles. (A) Viability of MCF-7 cells that incubated with different concentration of MSN (as the control group), FITC-MSN and **Ru@FITC-MSN** for 24 h, respectively. (B) Flow cytometry analysis of MCF-7 cells were incubated with different cellular uptake inhibitor, and then incubated with **Ru@FITC-MSN** (40 μg/mL) for 4 h (MFI, mean fluorescence intensity).

electrostatic interaction between negatively charged FITC-MSN and positively charged Ru(II) complexes. The TEM image of **Ru@FITC-MSN** shows spherical nanostructures with a similar diameter with FITC-MSN (Fig. 1B). The mesoporous structure was not changed, as reflected by SAXRD pattern (Fig. 1C). The C=C stretching peak in the FTIR spectrum was increased after Ru(II) loading (Fig. S1). The ζ-potential of **Ru@FITC-MSN** was increased to 14.9 mV in pure water due to the loading of positively charged $[Ru(bpy)_2(bpy\text{-}DPA)]^{2+}$. The $[Ru(bpy)_2(bpy\text{-}DPA)]^{2+}$ immobilization capacity was around 8 wt% determined by TGA (Fig. S2). The pore volume and the surface area of **Ru@FITC-MSN** was decreased to be 0.14 $cm^3\ g^{-1}$ and 64.5 $m^2\ g^{-1}$, respectively (Fig. 1D). These decrements clearly indicate the successful $[Ru(bpy)_2(bpy\text{-}DPA)]^{2+}$ loading into the mesoporous of FITC-MSN.

The association stability of FITC and Ru(II) complex in FITC-MSN and **Ru@FITC-MSN** was evaluated by measuring the changes of absorbance at 494 nm (FITC) and 456 nm (Ru(II) complex) in pure water, respectively. As shown in Fig. S3, more than 99% of FITC was associated with suspended FITC-MSN and 95% of $[Ru(bpy)_2(bpy\text{-}DPA)]^{2+}$ with **Ru@FITC-MSN** after 24 h incubation in pure water at room temperature, indicating the good association stability of two dye moieties in **Ru@FITC-MSN** in aqueous solution.

3.2. Ratiometric luminescence detection of H_2S in aqueous solution

Ru@FITC-MSN clearly showed two emission bands centred at 520 nm (FITC) and at 600 nm (Ru(II) complex) (Fig. S4). The dual emission nanoparticles allow ratiometric luminescence analysis using FTIC as the self-referenced channel and Ru(II) complex as the H_2S responsive channel. The luminescence response of **Ru@FITC-MSN** to Cu^{2+} was first investigated in HEPES buffer (pH 7.4). As shown in Fig. 2A, the luminescence emission of Ru(II) complex was remarkably quenched upon addition of Cu^{2+}, while the emission change of FITC was not observed. The ratiometric luminescence intensity (I_{520}/I_{600}) reached plateau after addition of 6 μM of Cu^{2+} (Fig. S5). The dose dependent luminescence intensity changes (I_{520}/I_{600}) displayed a good linearity in the range of 0.1–4 μM (Fig. S6), suggesting a quantitative quenching of Ru(II) emission after immobilized $[Ru(bpy)_2(bpy\text{-}DPA)]^{2+}$ binding to Cu^{2+}. Therefore, the **Ru–Cu@FITC-MSN** was prepared in-situ by adding Cu^{2+} into **Ru@FITC-MSN** aqueous solution.

To investigate the ratiometric luminescence response of as-prepared **Ru–Cu@FITC-MSN** to H_2S, a luminescence titration experiment was performed by adding different concentrations of H_2S to **Ru–Cu@FITC-MSN** in HEPES buffer (pH 7.4). As shown in Fig. 2B, the luminescence emission of Ru(II) complex was gradually increased while the emission of FITC was constant. The recovered luminescence spectrum was similar to the one of **Ru@FITC-MSN** (Fig. S4), suggesting effective displacement of Cu^{2+} by adding H_2S to turn on the red emission. Using unchanged FITC emission as the reference, ratiometric luminescence response (I_{600}/I_{520}) of **Ru–Cu@FITC-MSN** reached plateau after addition of 6 μM of H_2S (Fig. S7). The luminescence intensity ratio (I_{600}/I_{520}) showed a good linearity with the increased concentration of H_2S, as can be expressed as $I_{600}/I_{520} = 0.36 + 0.77\ [H_2S]$ (Fig. 2C). The detection limit (LoD) and quantification limit (LoQ) for H_2S were determined to be 0.36 and 1.21 μM, respectively. The LoD and LoQ of **Ru–Cu@FITC-MSN** are comparable to the previously reported method (Table S1), indicating that the H_2S can be quantitatively and sensitively detected using **Ru–Cu@FITC-MSN** nanosensor in this particular setting.

Fig. S8 illustrates the time-profile luminescence response of **Ru@FITC-MSN** to Cu^{2+} and in-situ generated **Ru–Cu@FITC-MSN** to H_2S in HEPES buffer. Upon addition of Cu^{2+}, the relative luminescence intensity of Ru(II) complex in **Ru@FITC-MSN** was rapidly decreased and the decreased luminescence intensity reached a steady level within 3 s. The luminescence quenching is attributed to the Cu^{2+}-mediated excited-state electron transfer and/or energy transfer of Ru(II) complex [46]. The relative luminescence intensity of Ru(II) complex was then rapidly increased upon addition of H_2S, and the maximum luminescence enhancement was observed within 5 s. These observations indicate that in-situ generated **Ru–Cu@FITC-MSN** nanosensor can rapidly detect H_2S in aqueous solution, which is one of the key requirements for a nanosensor to be used in detection of highly reactive biomarkers. Moreover, as shown in Fig. 2D, changes of luminescence intensity at 600 nm can be repeated more than 6 times upon addition of Cu^{2+}/H_2S, indicating that **Ru–Cu@FITC-MSN** nanosensor is reversible for H_2S detection [50].

The luminescence ratiometric response (I_{600}/I_{520}) of **Ru–Cu@FITC-MSN** showed high selectivity toward H_2S over other anions, ROS, RNS and biomolecules. As shown in Fig. 2E, the ratiometric value (I_{600}/I_{520}) of **Ru–Cu@FITC-MSN** was not obviously changed upon addition 50 μM of various anions, ROS, RNS and 1 mM of Cys, Hcy and GSH. This is in sharp contrast to H_2S at 6 μM that specifically reduced the ratiometric value (I_{600}/I_{520}) from 4.5 to 0.4 without influence from other competitive species. These data suggest that **Ru–Cu@FITC-MSN** is highly selective toward H_2S detection even in the presence of other species.

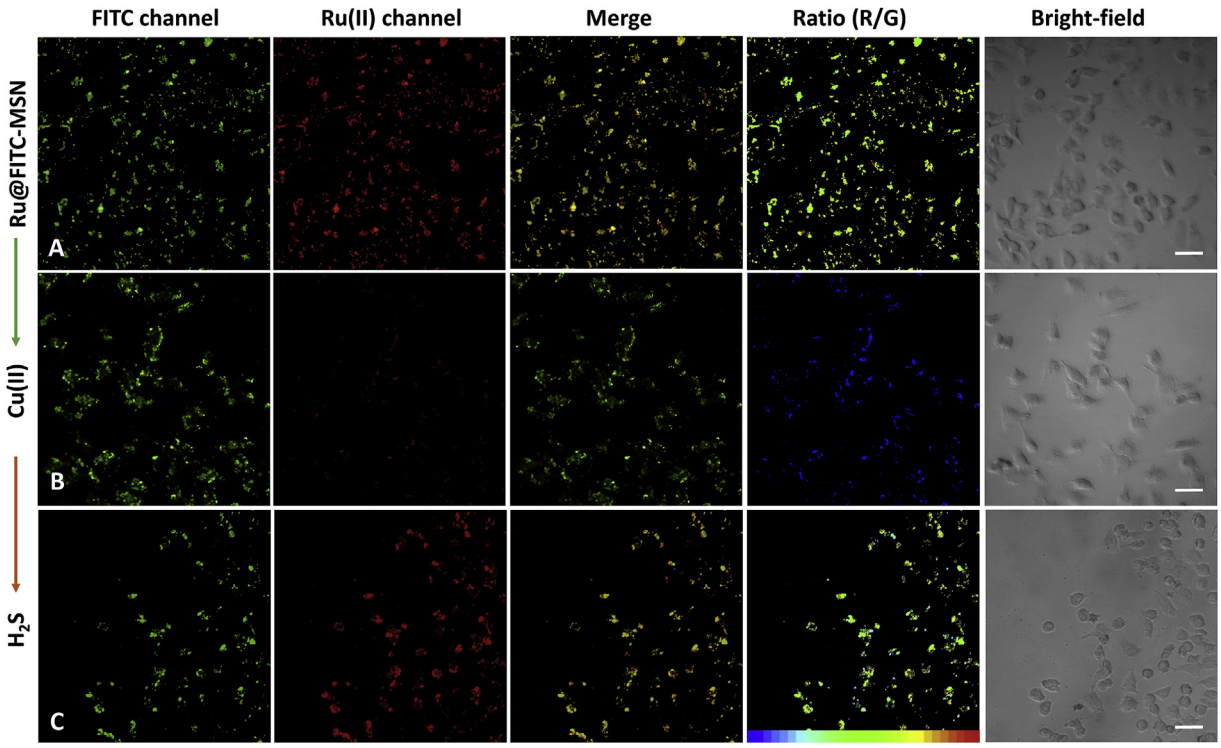

Fig. 4. Luminescence imaging of H_2S in live MCF-7 cells. The MCF-7 cells were incubated with **Ru@FITC-MSN** (40 μg/mL) for 4 h (A), and then the cells were treated with 20 μM Cu^{2+} for 30 min (B), followed by further treatment with H_2S for another 30 min (C). Scale bar, 50 μm.

3.3. Detection of H_2S in cells

The cytotoxicity of FITC-MSN and **Ru@FITC-MSN** towards breast cancer cell (MCF-7) was first evaluated by a standard 3-(4,5-dimethylthiazol-2-yl)-2,5-diphenyltetrazolium bromide (MTT) assay. As shown in Fig. 3A, the cell viability retained above 84% after incubating the cells at 40 μg/mL FITC-MSN and **Ru@FITC-MSN** for 24 h using MSN without FITC doping and Ru(II) complex immobilization as the reference, suggesting a low cytotoxicity of these nanoparticles in cell experiments at the concentration of 40 μg/mL [51].

MCF-7 cell uptake of **Ru@FITC-MSN** was next optimized through varying the nanoparticle concentration and the uptake time, with the intracellular signal expressed by means of mean fluorescence intensity (MFI) of flow cytometry analysis. As shown in Fig. S9, the intracellular MFI was increased upon incubation of MCF-7 cells with the increased concentration of the **Ru@FITC-MSN** (5–40 μg/mL). A very small change of MFI was obtained when at the higher concentration of **Ru@FITC-MSN** (40–100 μg/mL), suggesting that the optimized concentration of **Ru@FITC-MSN** is

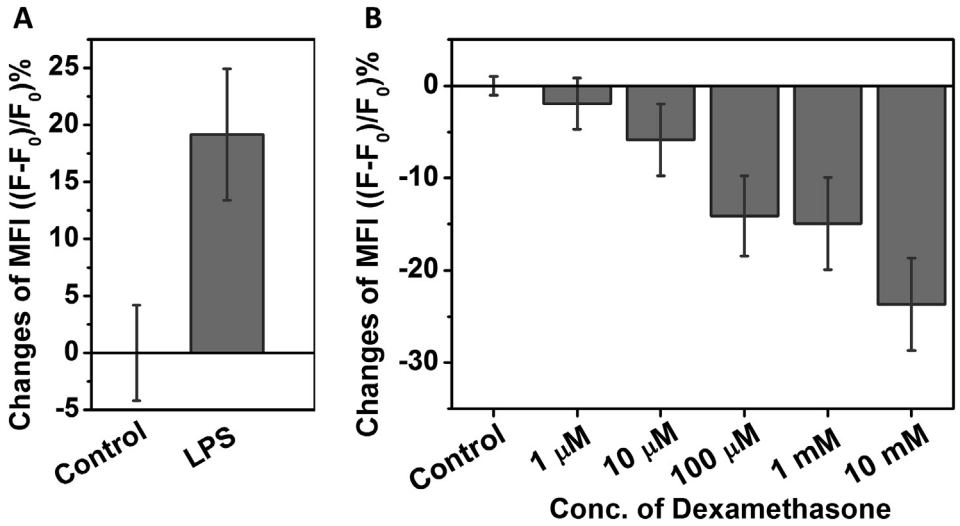

Fig. 5. Flow cytometry analysis of H_2S generation in inflammatory cancer cells. (A) MCF-7 cells were incubated with **Ru@FITC-MSN** (40 μg/mL) for 4 h, and then treated with Cu^{2+} (10 μM) for 30 min before stimulation with LPS (10 ng/mL) for 4 h. (B) MCF-7 cells were incubated with **Ru@FITC-MSN** (40 μg/mL) for 4 h, and then treated with Cu^{2+} (10 μM) for 30 min before stimulation with LPS (10 ng/mL) and dexamethasone (0, 1, 10, 100, 1000, and 10,000 μM) for 4 h.

possibly 40 μg/mL. The MCF-7 cells were then incubated with **Ru@FITC-MSN** (40 μg/mL) for 0.5, 1, 2, 4, and 8 h. As shown in Fig. S10, the intracellular MFI was gradually increased and the maximum MFI change was obtained after 4 h incubation, suggesting that the optimized cellular uptake time is possibly 4 h.

The potential cellular internalization pathway of **Ru@FITC-MSN** was further investigated following a previous method [52]. MCF-7 cells were incubated with **Ru@FITC-MSN** (40 μg/mL) for 4 h at 4 °C, and the intracellular MFI was measured by flow cytometer. Compared with the control group, the intracellular MFI of the MCF-7 cells incubated at 4 °C was significantly decreased (Fig. 3B), suggesting that **Ru@FITC-MSN** is internalized through an energy-dependent pathway. MCF-7 cells were pre-treated with various well-documented endocytosis inhibitor, followed by incubation with **Ru@FITC-MSN** (40 μg/mL) for 4 h. Significant decrease of MFI was not obtained when MCF-7 cells were pre-treated with filipin and colchicine, while the MFI of both FITC and Ru(II) channel was clearly decreased for the cells pre-treated with general endocytosis inhibitors (chloroquine and ammonium chloride) and nocodazole, suggesting the cellular internalization of **Ru@FITC-MSN** could be dominated by cell plasma membrane receptors and/or microtubules-mediated endocytosis.

Luminescence imaging of exogenous H_2S in MCF-7 cells were demonstrated by incubation of **Ru@FITC-MSN** for 4 h, followed by sequential treatment with Cu^{2+} and H_2S for 30 min. As shown in Fig. 4, the intracellular green luminescence in the FTIC channel was clearly observed and this signal was not changed during further sequential addition of Cu^{2+} and H_2S. Intense red emission in the Ru(II) complex channel was also noticed for MCF-7 cells incubated with **Ru@FITC-MSN** (Fig. 4A). Adding Cu^{2+} obviously diminished the intracellular red emission due to the formation of **Ru**–**Cu@FITC-MSN** (Fig. 4B), but the red luminescence signal was recovered upon further treatment with H_2S for 30 min (Fig. 4C). The "ON-OFF-ON" response in the Ru(II) channel led to yellow-green-yellow intracellular luminescence changes in merged images and green-blue-green ratiometric luminescence response in the ratio channel (R/G). Moreover, after incubation with the **Ru**–**Cu@FITC-MSN**, the cells showed weak luminescence in the Ru(II) complex channel (Fig. S11). Upon addition of exogenous H_2S, intracellular red luminescence signal was remarkably increased, suggesting the capability of intracellular H_2S detection in cancer cells.

The endogenous H_2S level in breast cancer cells was finally investigated by flow cytometry analysis. Activated bacterial cell wall component lipopolysaccharides (LPS) is a known activator that induces an inflammatory state of cells, including MCF-7 breast cancer cells [17,53,54], where H_2S is produced by increasing CSE expression [55,56]. Therefore, MCF-7 cells took up **Ru**–**Cu@FITC-MSN** for 4 h and were then treated with LPS. The intracellular luminescence intensity was recorded by flow cytometry analysis. As shown in Fig. 5A, the LPS-activated MCF-7 cells showed around 20% increase in the luminescence intensity, corresponding to the elevated expression of intracellular H_2S in the inflammatory state. Administering dexamethasone (an anti-inflammation drug) during LPS-activation decreased the intracellular MFI (Fig. 5B), suggesting the H_2S expression is inhibited. Moreover, corresponding decrease of H_2S expression also showed a dexamethasone concentration dependence, implying the efficiency of dexamethasone in the treatment of inflammation of cancer cells.

4. Conclusions

In conclusion, a new responsive luminescence nanosensor was developed for ratiometric luminescence detection of H_2S in aqueous solution and cells. The nanosensors were easily prepared by doping FITC to mesoporous silica nanoparticles and immobilizing Ru(II) complexes, $[Ru(bpy)_2(bpy\text{-}DPA)]^{2+}$ in the pores. The nanoparticles showed excellent colloid stability and dual emissions in aqueous solution. Adding Cu^{2+} then quenched the red luminescence and the in-situ generated nanosensors (**Ru**–**Cu@FITC-MSN**) enabled ratiometric luminescence detection of H_2S in aqueous solution using FITC as the reference. The cytotoxicity was limited and the cellular uptake pathway seemed to involve cell membrane receptors and microtubules-mediated endocytosis. The ratiometric luminescence imaging of H_2S was demonstrated, followed by the flow cytometry analysis of H_2S expression in inflammatory breast cancer cells and subsequent inhibition of H_2S generation upon the anti-inflammatory treatment. The present work provides a new approach for rapid and effective detection of H_2S.

Author contributions

R. Z and Z. P. X conceived the idea. J. L, C. D and R. Z per-formed the nanoparticles preparation and characterization. J. L, C. D, and H. T. T conducted the biological experiments. R. Z, W. Z and J. Y synthesized the ruthenium complexes. J. L and C. D wrote the original draft. R. Z and Z. P. X supervised the project, provided funding and resources, reviewed and edited the manuscript. All authors have given approval to the final version of the manuscript. J. L and C. D contributed equally to this work.

Declaration of competing interest

The authors declare that they have no known competing financial interests or personal relationships that could have appeared to influence the work reported in this paper.

Acknowledgments

The authors acknowledged the financial support by Australian Research Council (DE170100092, DP170104643, DP190103486) and the National Health and Medical Research Council (APP1125794). Facilities and assistance of Queensland Node of the Australian National Fabrication Facility (ANFF-Q), the University of Queensland, are also acknowledged.

Appendix A. Supplementary data

Supplementary data to this article can be found online at https://doi.org/10.1016/j.aca.2019.12.056.

References

[1] X. Chen, F. Wang, J.Y. Hyun, T. Wei, J. Qiang, X. Ren, I. Shin, J. Yoon, Recent progress in the development of fluorescent, luminescent and colorimetric probes for detection of reactive oxygen and nitrogen species, Chem. Soc. Rev. 45 (2016) 2976–3016.
[2] J. Chan, S.C. Dodani, C.J. Chang, Reaction-based small-molecule fluorescent probes for chemoselective bioimaging, Nat. Chem. 4 (2012) 973.
[3] C. Szabo, Gasotransmitters in cancer: from pathophysiology to experimental therapy, Nat. Rev. Drug Discov. 15 (2015) 185.
[4] N. Kumar, V. Bhalla, M. Kumar, Recent developments of fluorescent probes for the detection of gasotransmitters (NO, CO and H_2S), Coord. Chem. Rev. 257 (2013) 2335–2347.
[5] Q. Han, J. Liu, Q. Meng, Y.-L. Wang, H. Feng, Z. Zhang, Z.P. Xu, R. Zhang, Turn-on fluorescence probe for nitric oxide detection and bioimaging in live cells and zebrafish, ACS Sens. 4 (2019) 309–316.
[6] R. Kaushik, A. Ghosh, D. Amilan Jose, Recent progress in hydrogen sulphide (H2S) sensors by metal displacement approach, Coord. Chem. Rev. 347 (2017) 141–157.
[7] F. Yu, X. Han, L. Chen, Fluorescent probes for hydrogen sulfide detection and bioimaging, Chem. Commun. 50 (2014) 12234–12249.
[8] V.S. Lin, W. Chen, M. Xian, C.J. Chang, Chemical probes for molecular imaging and detection of hydrogen sulfide and reactive sulfur species in biological systems, Chem. Soc. Rev. 44 (2015) 4596–4618.

[9] C. Zhao, X. Zhang, K. Li, S. Zhu, Z. Guo, L. Zhang, F. Wang, Q. Fei, S. Luo, P. Shi, H. Tian, W.-H. Zhu, Förster resonance energy transfer switchable self-assembled micellar nanoprobe: ratiometric fluorescent trapping of endogenous H2S generation via fluvastatin-stimulated upregulation, J. Am. Chem. Soc. 137 (2015) 8490–8498.

[10] Y.L. Pak, J. Li, K.C. Ko, G. Kim, J.Y. Lee, J. Yoon, Mitochondria-targeted reaction-based fluorescent probe for hydrogen sulfide, Anal. Chem. 88 (2016) 5476–5481.

[11] D. Qiao, T. Shen, M. Zhu, X. Liang, L. Zhang, Z. Yin, B. Wang, L. Shang, A highly selective and sensitive fluorescent probe for simultaneously distinguishing and sequentially detecting H2S and various thiol species in solution and in live cells, Chem. Commun. 54 (2018) 13252–13255.

[12] C. Wang, X. Cheng, J. Tan, Z. Ding, W. Wang, D. Yuan, G. Li, H. Zhang, X. Zhang, Reductive cleavage of C-C bonds as a new strategy for turn-on dual fluorescence in effective sensing of H_2S, Chem. Sci. 9 (2018) 8369–8374.

[13] S. Wang, S. Xu, G. Hu, X. Bai, T.D. James, L. Wang, A fluorescent chemodosimeter for live-cell monitoring of aqueous sulfides, Anal. Chem. 88 (2016) 1434–1439.

[14] L. Wei, Z. Zhu, Y. Li, L. Yi, Z. Xi, A highly selective and fast-response fluorescent probe for visualization of enzymatic H2S production in vitro and in living cells, Chem. Commun. 51 (2015) 10463–10466.

[15] R. Zhang, B. Song, J. Yuan, Bioanalytical methods for hypochlorous acid detection: recent advances and challenges, TrAC Trends Anal. Chem. (Reference Ed.) 99 (2018) 1–33.

[16] Y.J. Jang, K. Kim, O.G. Tsay, D.A. Atwood, D.G. Churchill, Update 1 of: destruction and detection of chemical warfare agents, Chem. Rev. 115 (2015) PR1–PR76.

[17] Z. Du, B. Song, W. Zhang, C. Duan, Y.-L. Wang, C. Liu, R. Zhang, J. Yuan, Quantitative monitoring and visualization of hydrogen sulfide In Vivo using a luminescent probe based on a ruthenium(II) complex, Angew. Chem. Int. Ed. 57 (2018) 3999–4004.

[18] W. Zhang, J. Kang, P. Li, H. Wang, B. Tang, Dual signaling molecule sensor for rapid detection of hydrogen sulfide based on modified tetraphenylethylene, Anal. Chem. 87 (2015) 8964–8969.

[19] Q. Han, Z. Mou, H. Wang, X. Tang, Z. Dong, L. Wang, X. Dong, W. Liu, Highly selective and sensitive one- and two-photon ratiometric fluorescent probe for intracellular hydrogen polysulfide sensing, Anal. Chem. 88 (2016) 7206–7212.

[20] C. Zhang, L. Wei, C. Wei, J. Zhang, R. Wang, Z. Xi, L. Yi, A FRET–ICT dual-quenching fluorescent probe with large off–on response for H2S: synthesis, spectra and bioimaging, Chem. Commun. 51 (2015) 7505–7508.

[21] L. Yang, Y. Su, Y. Geng, Y. Zhang, X. Ren, L. He, X. Song, A triple-emission fluorescent probe for discriminatory detection of cysteine/homocysteine, glutathione/hydrogen sulfide, and thiophenol in living cells, ACS Sens. 3 (2018) 1863–1869.

[22] M.D. Hammers, M.J. Taormina, M.M. Cerda, L.A. Montoya, D.T. Seidenkranz, R. Parthasarathy, M.D. Pluth, A bright fluorescent probe for H_2S enables analyte-responsive, 3D imaging in live zebrafish using light sheet fluorescence microscopy, J. Am. Chem. Soc. 137 (2015) 10216–10223.

[23] S.-J. Li, Y.-F. Li, H.-W. Liu, D.-Y. Zhou, W.-L. Jiang, J. Ou-Yang, C.-Y. Li, A dual-response fluorescent probe for the detection of viscosity and H_2S and its application in studying their cross-talk influence in mitochondria, Anal. Chem. 90 (2018) 9418–9425.

[24] N. Gupta, S.I. Reja, V. Bhalla, M. Gupta, G. Kaur, M. Kumar, A bodipy based dual functional probe for the detection of hydrogen sulfide and H_2S induced apoptosis in cellular systems, Chem. Commun. 51 (2015) 10875–10878.

[25] C. Wei, R. Wang, L. Wei, L. Cheng, Z. Li, Z. Xi, L., Yi o-Fluorination of aromatic azides yields improved azido-based fluorescent probes for hydrogen sulfide: synthesis, spectra, and bioimaging, Chem. Asian J. 9 (2014) 3586–3592.

[26] Y. Yan, H. Yu, Y. Zhang, K. Zhang, H. Zhu, T. Yu, H. Jiang, S. Wang, Molecularly engineered quantum dots for visualization of hydrogen sulfide, ACS Appl. Mater. Interfaces 7 (2015) 3547–3553.

[27] D.-T. Shi, D. Zhou, Y. Zang, J. Li, G.-R. Chen, T.D. James, X.-P. He, H. Tian, Selective fluorogenic imaging of hepatocellular H2S by a galactosyl azido-naphthalimide probe, Chem. Commun. 51 (2015) 3653–3655.

[28] S. Yang, Y. Qi, C. Liu, Y. Wang, Y. Zhao, L. Wang, J. Li, W. Tan, R. Yang, Design of a simultaneous target and location-activatable fluorescent probe for visualizing hydrogen sulfide in lysosomes, Anal. Chem. 86 (2014) 7508–7515.

[29] L.A. Montoya, M.D. Pluth, Organelle-targeted H_2S probes enable visualization of the subcellular distribution of H2S donors, Anal. Chem. 88 (2016) 5769–5774.

[30] N. Adarsh, M.S. Krishnan, D. Ramaiah, Sensitive naked eye detection of hydrogen sulfide and nitric oxide by aza-BODIPY dyes in aqueous Medium, Anal. Chem. 86 (2014) 9335–9342.

[31] A. Ji, Y. Fan, W. Ren, S. Zhang, H.-w. Ai, A sensitive near-infrared fluorescent sensor for mitochondrial hydrogen sulfide, ACS Sens. 3 (2018) 992–997.

[32] Y. Qian, J. Karpus, O. Kabil, S.-Y. Zhang, H.-L. Zhu, R. Banerjee, J. Zhao, C. He, Selective fluorescent probes for live-cell monitoring of sulphide, Nat. Commun. 2 (2011) 495.

[33] S. Singha, D. Kim, H. Moon, T. Wang, K.H. Kim, Y.H. Shin, J. Jung, E. Seo, S.-J. Lee, K.H. Ahn, Toward a selective, sensitive, fast-responsive, and biocompatible two-photon probe for hydrogen sulfide in live cells, Anal. Chem. 87 (2015) 1188–1195.

[34] J. Liu, X. Guo, R. Hu, X. Liu, S. Wang, S. Li, Y. Li, G. Yang, Molecular engineering of aqueous soluble triarylboron-compound-based two-photon fluorescent probe for mitochondria H2S with analyte-induced finite aggregation and excellent membrane permeability, Anal. Chem. 88 (2016) 1052–1057.

[35] M. Sun, H. Yu, H. Li, H. Xu, D. Huang, S. Wang, Fluorescence signaling of hydrogen sulfide in broad pH range using a copper complex based on BINOL–benzimidazole ligands, Inorg. Chem. 54 (2015) 3766–3772.

[36] X. Qu, C. Li, H. Chen, J. Mack, Z. Guo, Z. Shen, A red fluorescent turn-on probe for hydrogen sulfide and its application in living cells, Chem. Commun. 49 (2013) 7510–7512.

[37] Q. Meng, Y. Shi, C. Wang, H. Jia, X. Gao, R. Zhang, Y. Wang, Z. Zhang, NBD-based fluorescent chemosensor for the selective quantification of copper and sulfide in an aqueous solution and living cells, Org. Biomol. Chem. 13 (2015) 2918–2926.

[38] R. Kaushik, R. Sakla, A. Ghosh, G.T. Selvan, P.M. Selvakumar, D.A. Jose, Selective detection of H_2S by copper complex embedded in vesicles through metal indicator displacement approach, ACS Sens. 3 (2018) 1142–1148.

[39] Q. Yu, K.Y. Zhang, H. Liang, Q. Zhao, T. Yang, S. Liu, C. Zhang, Z. Shi, W. Xu, W. Huang, Dual-emissive nanohybrid for ratiometric luminescence and lifetime imaging of intracellular hydrogen sulfide, ACS Appl. Mater. Interfaces 7 (2015) 5462–5470.

[40] E. Karakuş, M. Üçüncü, M. Emrullahoğlu, Electrophilic cyanate as a recognition motif for reactive sulfur species: selective fluorescence detection of H_2S, Anal. Chem. 88 (2016) 1039–1043.

[41] B. Peng, W. Chen, C. Liu, E.W. Rosser, A. Pacheco, Y. Zhao, H.C. Aguilar, M. Xian, Fluorescent probes based on nucleophilic substitution–cyclization for hydrogen sulfide detection and bioimaging, Chem. Eur J. 20 (2014) 1010–1016.

[42] J. Zhang, Y.-Q. Sun, J. Liu, Y. Shi, W. Guo, A fluorescent probe for the biological signaling molecule H2S based on a specific H_2S trap group, Chem. Commun. 49 (2013) 11305–11307.

[43] G. Jiang, M. Li, Y. Wen, W. Zeng, Q. Zhao, C. Chen, H. Yuan, C. Liu, C. Liu, Visualization of sulfane sulfur in plants with a near-infrared fluorescent probe, ACS Sens. 4 (2019) 434–440.

[44] D. Andina, J.-C. Leroux, P. Luciani, Ratiometric fluorescent probes for the detection of reactive oxygen species, Chem. Eur J. 23 (2017) 13549–13573.

[45] Y. Li, X. Zhang, B. Zhu, J. Xue, Z. Zhu, W. Tan, A simple but highly sensitive and selective colorimetric and fluorescent probe for Cu^{2+} in aqueous media, Analyst 136 (2011) 1124–1128.

[46] R. Zhang, X. Yu, Y. Yin, Z. Ye, G. Wang, J. Yuan, Development of a hetero-bimetallic Ru(II)–Cu(II) complex for highly selective and sensitive luminescence sensing of sulfide anions, Anal. Chim. Acta 691 (2011) 83–88.

[47] A. Imhof, M. Megens, J.J. Engelberts, D.T.N. de Lang, R. Sprik, W.L. Vos, Spectroscopy of fluorescein (FITC) dyed colloidal silica spheres, J. Phys. Chem. B 103 (1999) 1408–1415.

[48] L. Yang, Y. Chen, Z. Yu, W. Pan, H. Wang, N. Li, B. Tang, Dual-ratiometric fluorescent nanoprobe for visualizing the dynamic process of pH and superoxide anion changes in autophagy and apoptosis, ACS Appl. Mater. Interfaces 9 (2017) 27512–27521.

[49] Z. Chen, P. Yan, L. Zou, M. Zhao, J. Jiang, S. Liu, K.Y. Zhang, W. Huang, Q. Zhao, Using ultrafast responsive phosphorescent nanoprobe to visualize elevated peroxynitrite in vitro and in vivo via ratiometric and time-resolved photoluminescence imaging, Adv. Healthc. Mater. 7 (2018) 1800309.

[50] Z. Ji, Y. Cheng, X. Cui, H. Lin, J. Xu, Y. Wang, Heating-induced abnormal increase in Yb^{3+} excited state lifetime and its potential application in lifetime luminescence nanothermometry, Inorg. Chem. Front. 6 (2019) 110–116.

[51] A. Aysun, K. Yağmur, B. Yusuf, Cell proliferation and cytotoxicity assays, Curr. Pharmaceut. Biotechnol. 17 (2016) 1213–1221.

[52] L. Cao, R. Zhang, W. Zhang, Z. Du, C. Liu, Z. Ye, B. Song, J. Yuan, A ruthenium(II) complex-based lysosome-targetable multisignal chemosensor for in vivo detection of hypochlorous acid, Biomaterials 68 (2015) 21–31.

[53] Z.W. Lee, J. Zhou, C.-S. Chen, Y. Zhao, C.-H. Tan, L. Li, P.K. Moore, L.-W. Deng, The slow-releasing hydrogen sulfide donor, GYY4137, exhibits novel anti-cancer effects in vitro and in vivo, PLoS One 6 (2011), e21077.

[54] Z. Du, R. Zhang, B. Song, W. Zhang, Y.-L. Wang, J. Liu, C. Liu, Z.P. Xu, J. Yuan, Iridium(III) complex-based activatable probe for phosphorescent/time-gated luminescent sensing and imaging of cysteine in mitochondria of live cells and animals, chem, Eur. J. 25 (2019) 1498–1506.

[55] S.I. Reja, N. Sharma, M. Gupta, P. Bajaj, V. Bhalla, R.D. Parihar, P. Ohri, G. Kaur, M. Kumar, A highly selective fluorescent probe for detection of hydrogen sulfide in living systems: in vitro and in vivo applications, Chem. Eur J. 23 (2017) 9872–9878.

[56] L.-F. Hu, M. Lu, P.T.H. Wong, J.-S. Bian, Hydrogen sulfide: neurophysiology and neuropathology, antioxid, Redox Signal 15 (2011) 405–419.

Supplementary Materials for

Responsive Nanosensor for Ratiometric Luminescence Detection of Hydrogen Sulfide in Inflammatory Cancer Cells

Jianping Liu,[a,1] Chengchen Duan,[a,1] Wenzhu Zhang,[b] Hang Thu Ta,[a,c] Jingli Yuan,[b] Run Zhang,[a,*] Zhi Ping Xu[a,*]

[a] Australian Institute for Bioengineering and Nanotechnology (AIBN), The University of Queensland, Brisbane 4072, Australia

[b] State Key Laboratory of Fine Chemicals, School of Chemistry, Dalian University of Technology, Dalian 116024, China

[c] School of Pharmacy, University of Queensland, Woollongabba, QLD 4102, Australia

* Corresponding authors.

Email: r.zhang@uq.edu.au (R. Zhang), gordonxu@uq.edu.au (Z. P. Xu)

[1] These authors contributed equally to this work.

General information

General procedure for spectroscopic analysis

Stock solution of **Ru@FITC-MSN** (1 mg/mL) and **Ru-Cu@FITC-MSN** (1 mg/mL) were prepared in water. Before spectroscopic measurements, the solution was freshly prepared by diluting the stock solution to HEPES buffer (pH 7.4) to the corresponding solution at the concentration of 50 μg/mL. The solution of H_2S (NaHS as the donor) was then added to the solution (total volume 3.0 mL), and then the solution was mixed at R.T. for 5 min before the spectroscopic analysis. Excitation and emission slits are 5 nm.

Preparation of reactive oxygen species (ROS) and ions

Solutions of a series of anions (20 mM) were freshly prepared by dissolving corresponding chemicals in deionized water. A stock solution of HOCl was prepared by dilution of the commercial sodium hypochlorite solution and stored according to the previous literatures [1]. The concentration of HOCl was determined by using its molar extinction coefficient of 391 $M^{-1}cm^{-1}$ at 292 nm before use [2]. Hydroxyl radical (·OH) was generated in the Fenton system from ferrous ammonium sulfate and hydrogen peroxide [3]. Superoxide anion radical (O_2^-) was generated from the xanthine-xanthine oxidase system [4]. $ONOO^-$ was donated by 3-morpholinosydnonimine (SIN-1) [5]. Nitric oxide was generated by 1-hydroxy-2-oxo-3-(3-aminopropyl)-3-methyl-1-triazene (NOC-13) [6]. Hydrogen peroxide (H_2O_2) was diluted immediately from a stabilized 30% solution, and was assayed using its molar absorption coefficient of 43.6 $M^{-1}cm^{-1}$ at 240 nm [7]. Anhydrous sodium hydrosulfide (NaHS) was used as the donor of H_2S [8]. The NaHS water solution was freshly prepared and used for all experiments.

Cell line and cell culture

Human breast cancer cell line, MCF-7 (ATCC® HTB-22™) was obtained from American Type Cell Collection. MCF-7 cells were cultured in DMEM, supplemented with 10% FBS, 1% penicillin, 1% streptomycin sulfate in a humidified 5% CO_2/95% air incubator at 37 ºC. The growth medium was

changed every two days. MCF-7 cells were routinely subcultured with trypsin-EDTA solution and growth to 80% confluence prior to experiments.

Cell viability assays

The cytotoxicity of **Ru@FITC-MSN** toward MCF-7 cells was examined by MTT assay method. This assay involves the reduction of a yellow tetrazolium salt, [3-(4,5-dimethylthazol-2-yl)-2,5-diphenyltetrazolium bromide] tetrazolium to insoluble formazan crystals by the metabolic activity of live MCF-7 cells. MCF-7 cells were seeded at a density of 5×10^4 cells/mL in a 96-well micro-assay culture plate. After growth at 37 ^oC in a 5% CO_2 incubator for 24 h, the culture medium was replaced with the freshly prepared medium containing different concentrations of **Ru@FITC-MSN** (0, 5, 10, 20, 40 and 100 μg/mL). The group with the addition of culture medium only was employed as the control, and the wells containing culture media without cells were used as blanks. After incubation at 37 ^oC in a 5% CO_2 incubator for 24 h, cell culture medium was removed and cells were carefully washed three times with PBS. Then, the MTT solution in PBS (100 μL, 0.5 mg/mL) was added to each well for further incubation for 4 h. The excess MTT solution was then carefully removed from each well, and the formed formazan was dissolved in 100 μL of dimethyl sulfoxide (DMSO). The absorbance at 570 nm was measured in an Infinite M200 Pro Microplate Reader. The results from the five individual experiments were averaged. The following formula was used to calculate the viability of cell growth:

Vialibity (%) = (mean of absorbance value of treatment group-blank)/(mean absorbance value of control-blank) × 100.

All of the measurements were performed five times and the values are presented as the mean ± SD.

Confocal luminescence imaging in cells

Confocal luminescence imaging of both green channel (FITC channel) and red channel (Ru(II) channel) was performed to investigate the capability of nanosensor for sensing of H_2S. MCF-7 were typically seeded at a density of 3×10^5 cells/mL in a cell culture dish (ϕ = 20 mm) for the

luminescence microscopic cell imaging. After incubation for 24 h, the culture medium was replaced with the freshly prepared medium containing **Ru@FITC-MSN** (40 μg/mL), and the cells were further incubated at 37 °C in a 5% CO_2/95% air incubator for 4 h. The excess **Ru@FITC-MSN** was then removed, and the cells were washed with PBS for three times. Then, following experiments were designed and performed:

a) Cells were treated with 20 μM Cu^{2+} in PBS;

b) Group (a) cells were washed with PBS for three times and then supplied with 20 μM H_2S (NaHS as the donor).

Flow cytometry analysis

The cellular uptake and the detection of H_2S production in live cells were investigated by flow cytometry analysis. All of the measurements were performed three times and the values are presented as the means ± SD. Details of experiments include:

a) Concentration-dependent cellular uptake

MCF-7 cells were seeded into the wells of a six-well cell culture plate at the density of 1×10^5 cells/mL. After 24 h, the cell culture medium was replaced with the freshly prepared medium containing 0, 5, 10, 20, 40, 50, 75, 100 μg/mL **Ru@FITC-MSN**. The cells were incubated at 37 ºC for 4 h and then washed with PBS for three times to remove excess **Ru@FITC-MSN**. Then cells were detached and collected for flow cytometry analysis.

b) Time-dependent cellular uptake

MCF-7 cells were seeded into the wells of a six-well cell culture plate at the density of 1×10^5 cells/mL. After 24 h, the cell culture medium was replaced with the freshly prepared medium containing 40 μg/mL **Ru@FITC-MSN** (control group: cell culture medium without **Ru@FITC-MSN** was added). The cells were further incubated for 0.5, 1, 2, 4, and 8 h. After washing with PBS

for three times, the cells were detached by incubation with 0.25% EDTA-Trypsin and then collected by centrifugation.

c) Cellular internalization pathway

The cellular uptake pathway of sensor was investigated by flow cytometry analysis after treating with different endocytic inhibitors. MCF-7 cells were seeded into a six-well plate at the density of 1×10^5 cells/mL. After 24 h incubation at 37 ^oC, cell culture medium was replaced with freshly prepared medium containing chloroquine (100 μM), filipin (10 μg/mL), nocodazole (10 μM), colchicine (10 μM), NH_4Cl (10 mM), respectively. Then, **Ru@FITC-MSN** (40 μg/mL) was added into the medium of each well and the cells were further incubated for another 4 h. After washing with PBS for three times to remove excess **Ru@FITC-MSN**, the cells were detached by incubation with 0.25% EDTA-trypsin and collected by centrifugation.

For cells incubation at reduced temperature, the MCF-7 cells were keep at 4 ^oC for 30 min, and the cell culture medium was replaced with cold fresh medium containing **Ru@FITC-MSN** (40 μg/mL) followed by incubation at 4 ^oC for another 4 h. After washing with cold PBS for three times to remove excess **Ru@FITC-MSN**, the cells were detached by incubation with 0.25% EDTA-trypsin and collected by centrifugation for flow cytometry analysis.

d) Quantification of H_2S generation in MCF-7 cells

MCF-7 were seeded into 6-well plate at the density of 5×10^5 cells/well. After 24 h incubation at 37 ^oC, three group experiments were designed and performed:

i) Cells were further incubated at 37 ^oC for another 7 h a as the blank;

ii) Cells were incubated at 37 ^oC for 4 h and then incubated with **Ru@FITC-MSN** (40 μg/mL) for another 4 h followed by treatment with 20 μM Cu^{2+};

iii) Group (ii) cells were treated with LPS (10 ng/mL) for 4 h;

iv) Group (ii) cells were incubated with LPS (10 ng/mL) and dexamethasone at different concentrations (0, 1, 10, 100, 10^3, and 10^4 μM).

The cells of each group were washed with PBS for three times and then detached and collected for flow cytometry analysis.

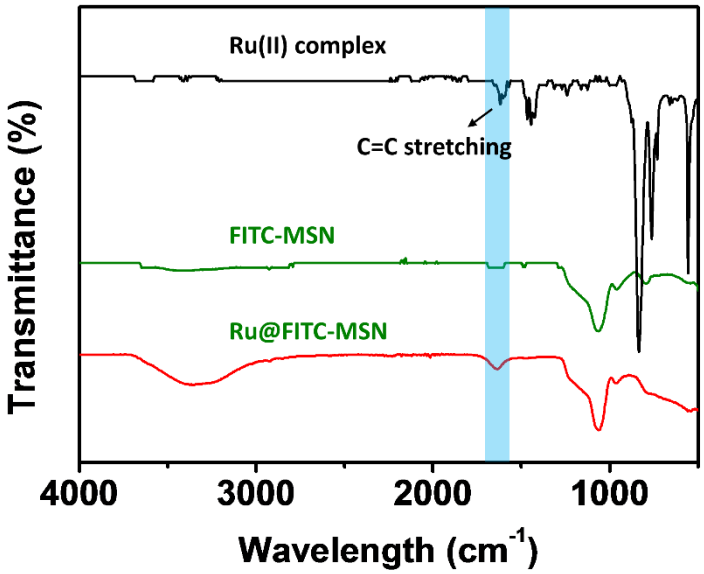

Figure S1. FTIR of Ru(II) complex, FITC-MSN and Ru@FITC-MSN.

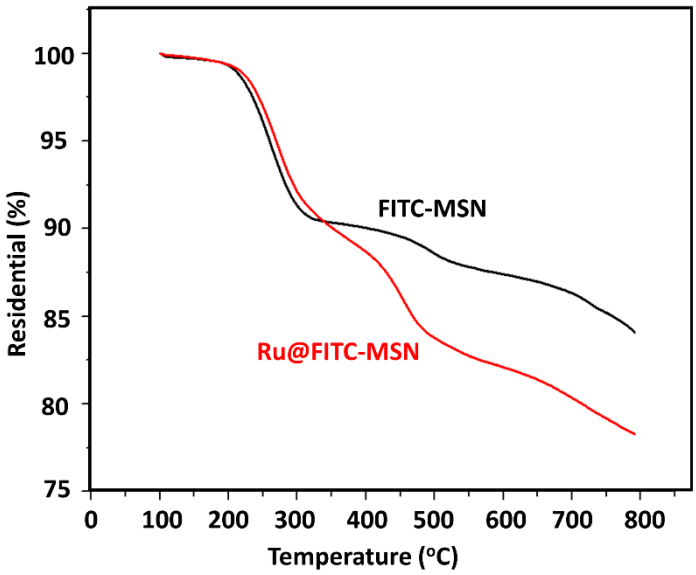

Figure S2. Thermogravimetric analysis of FITC-MSN and Ru@FITC-MSN.

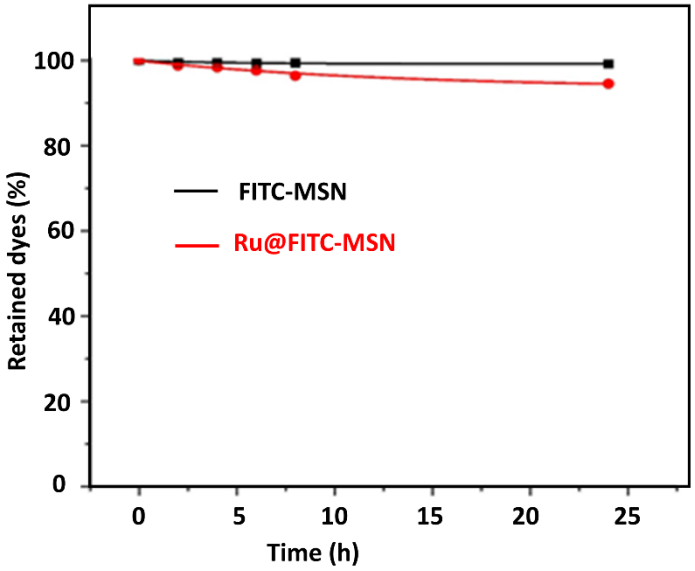

Figure S3. Stability of FITC-MSN and Ru@FITC-MSN in aqueous solution.

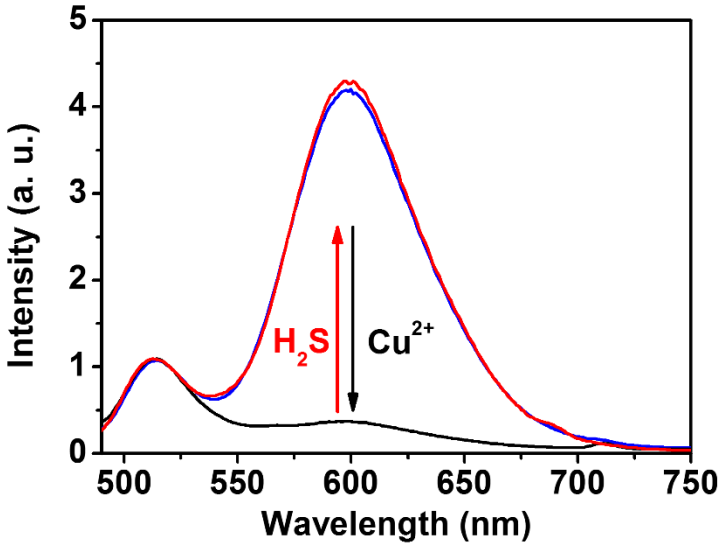

Figure S4. Emission spectra of Ru@FITC-MSN (red line), in-situ generated Ru-Cu@FITC-MSN in the absence (black line) and presence of H_2S (blue line).

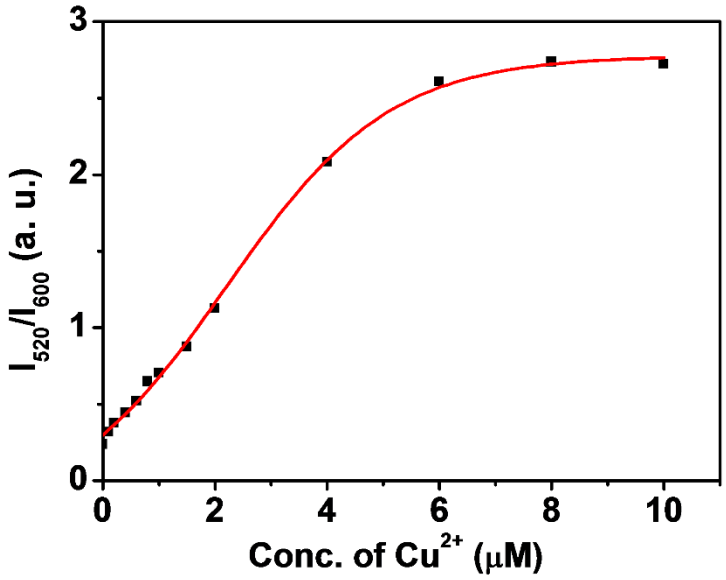

Figure S5. Ratiometric emission intensity changes (I_{520}/I_{600}) of **Ru@FITC-MSN** in the presence of Cu^{2+} at concentrations of 0, 0.2, 0.4, 0.8, 1, 1.5, 2, 4, 6, 8, and 10 μM.

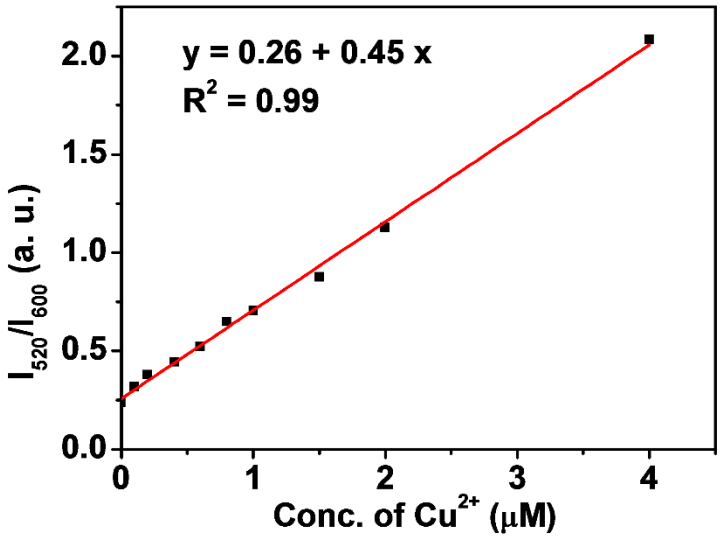

Figure S6. Linearity of ratiometric emission intensity changes (I_{520}/I_{600}) against the concentration of Cu^{2+}.

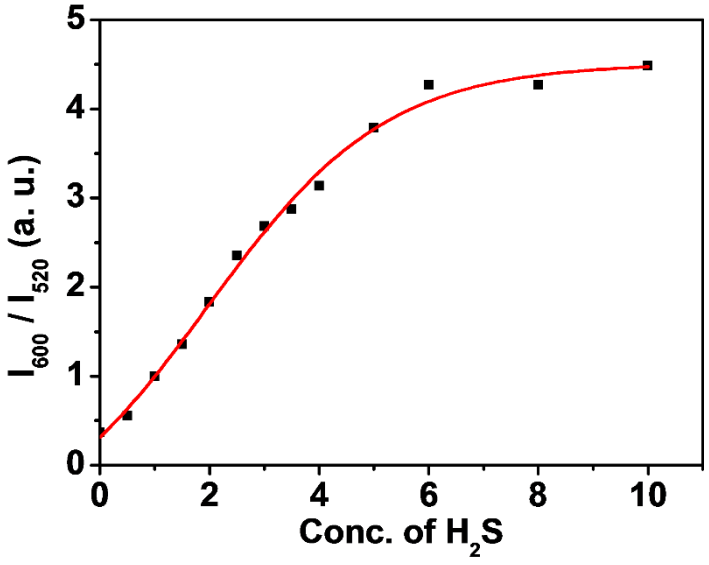

Figure S7. Ratiometric changes of luminescence emission intensity (I_{600}/I_{520}) upon H_2S addition to **Ru-Cu@FITC-MSN**.

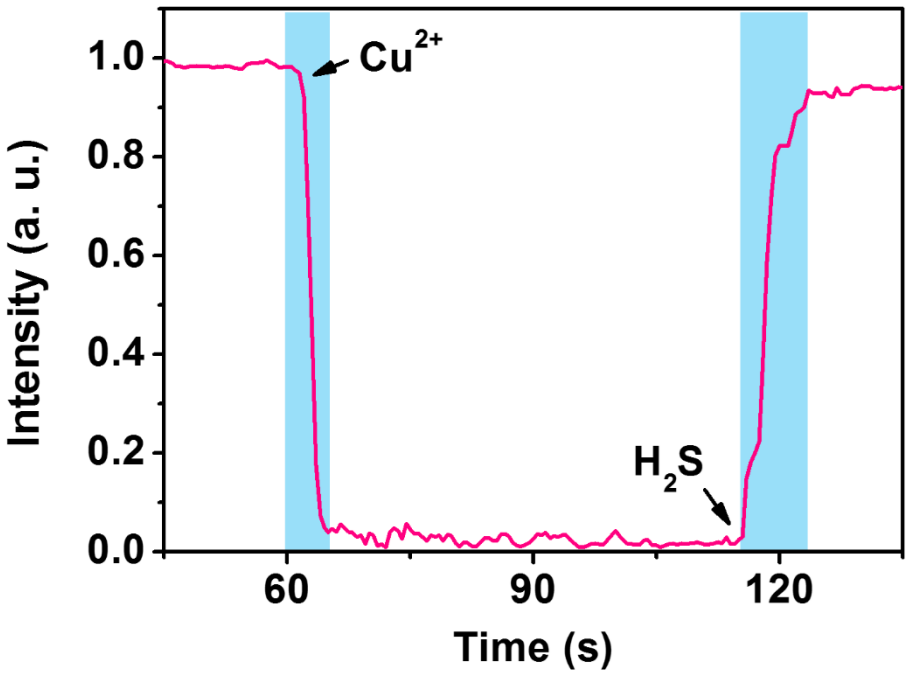

Figure S8. Time course luminescence intensity (λ_{ex} = 450 nm, λ_{em} = 600 nm) changes of **Ru@FITC-MSN** response to Cu^{2+} addition and in-situ produced **Ru-Cu@FITC-MSN** response to H_2S.

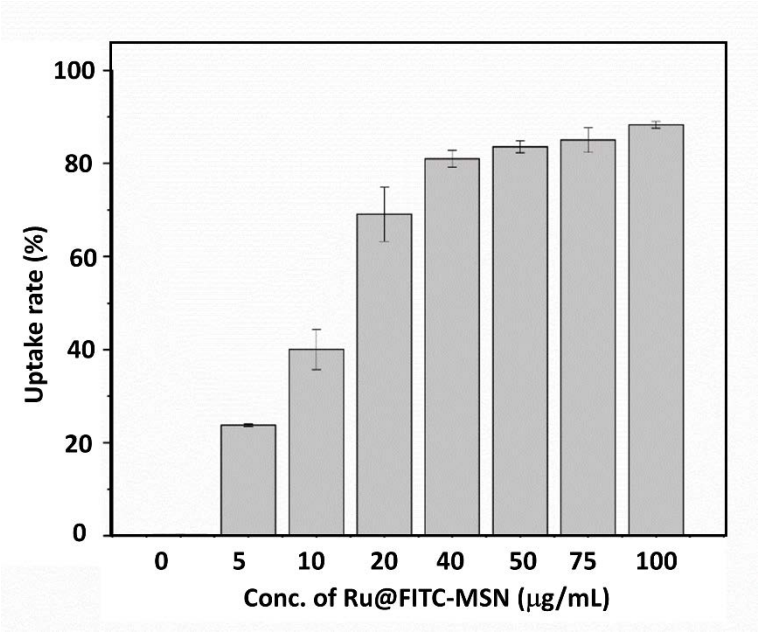

Figure S9. Flow cytometry analysis of cellular uptake rate of Ru@FITC-MSN at different concentration (0, 5, 10, 20, 40, 50, 75, and 100 μg/mL) in 4 h incubation.

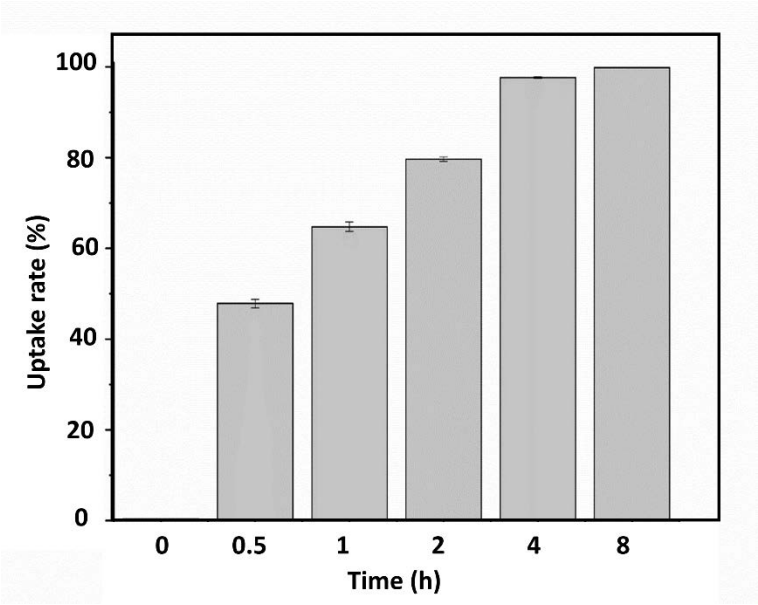

Figure S10. Flow cytometry analysis of cellular uptake rate of **Ru@FITC-MSN** (40 μg/mL) in different time incubation (0, 0.5, 1, 2, 4, and 8 h).

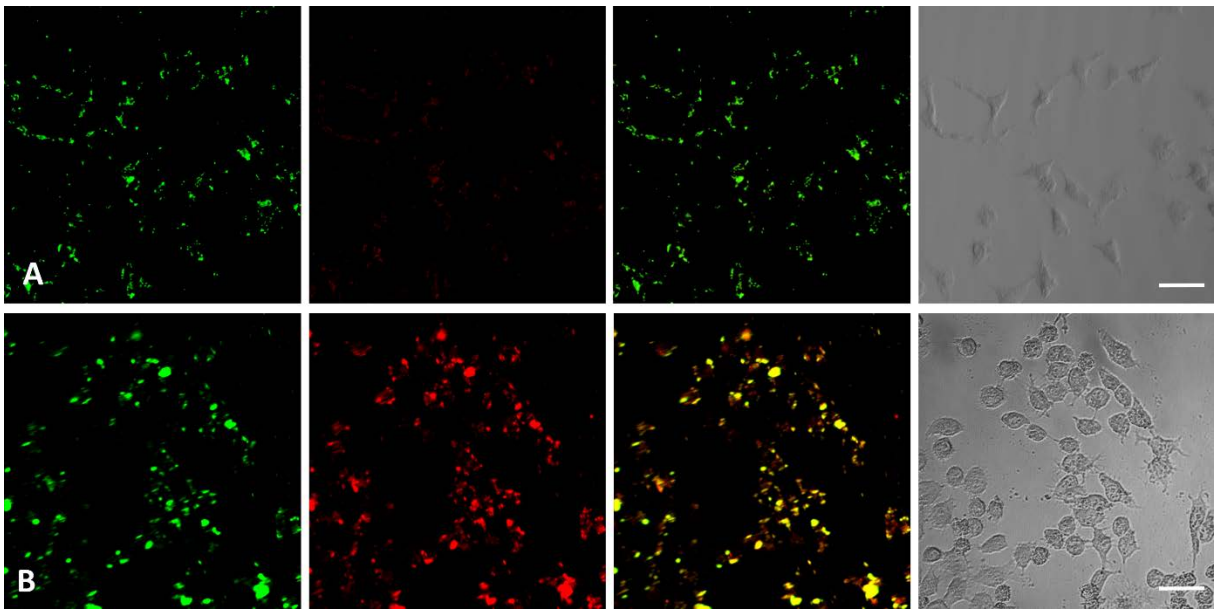

Figure S11. Luminescence imaging of H_2S in MCF-7 cells. The MCF-7 cells were incubated with **Ru-Cu@FITC-MSN** (40 μg/mL) (A) for 4 h, and then treated with H_2S (B) for another 30 min. Scale bar, 50 μm.

Table S1. Summary and comparison of the proposed protocol with other reported methods for H_2S detection

Method	Name	$\lambda_{ex}/\lambda_{em}$ (nm)	LoD	LoQ	Linearity range	Response time	Biological applications	Ref.
OFF-ON	Ru-MDB	450/612	45 nM	-	0-80 μM	50 min	H_2S imaging in cells, zebrafish and mice	[9]
	TPE-NP	405/480	12.8 nM	-	0.1 μM-0.8 mM	Instant	H_2S imaging in cells and *C.elegans*	[10]
	1	405/455	0.28 μM	-	0-100 μM	Overnight	H_2S imaging in cells	[11]
	NCQ	423/490	0.52 μM	-	0-8 μM	15 min	H_2S imaging in cells	[12]
	MeRho-Az	476/516	86 nM	-	0-15 μM	> 120 min	H_2S imaging in zebrafish	[8]
	Mito-VS	370/510	0.17 μM	-	0.5-100 μM	30 min	H_2S imaging in cells	[13]
	7b	350/450	0.61 μM	-	0-150 μM	40 min	H_2S imaging in cells	[14]
	DT-Gal	426/-	0.78 μM	-	0-90 μM	-	H_2S imaging in cells	[15]
	SulpHensor	530/555	0.5 μM	-	0-10 μM	> 60 min	H_2S imaging in cells	[16]
	P3	375/-	50 nM	-	0.1-50 μM	10 min	H_2S imaging in cells	[17]
ON-OFF	1	470/515	35 nM	-	< 35 μM	20 min	H_2S imaging in cells	[18]
	3a	560/750	14.7 μM	-	1.3-1.8 μM	-	-	[19]
Ratiometric		-/452,657	7 nM	-	0-2 μM	15 min	-	[20]
	Ru-Cu@FITC-MSN	450/520, 600	0.36 μM	1.21 μM	0-4 μM	< 5 s	H_2S imaging and flow cytometry analysis in inflammatory cancer cells and tracking cancer cell treatment	This work

References

[1] F. Zhang, X. Liang, W. Zhang, Y.-L. Wang, H. Wang, Y.H. Mohammed, B. Song, R. Zhang, J. Yuan, A unique iridium(III) complex-based chemosensor for multi-signal detection and multi-channel imaging of hypochlorous acid in liver injury, Biosensors and Bioelectronics, 87 (2017) 1005-1011.

[2] S. Chen, J. Lu, C. Sun, H. Ma, A highly specific ferrocene-based fluorescent probe for hypochlorous acid and its application to cell imaging, Analyst, 135 (2010) 577-582.

[3] X. Bai, Y. Huang, M. Lu, D. Yang, HKOH-1: A Highly Sensitive and Selective Fluorescent Probe for Detecting Endogenous Hydroxyl Radicals in Living Cells, Angewandte Chemie International Edition, 56 (2017) 12873-12877.

[4] X. Lu, Z. Chen, X. Dong, W. Zhao, Water-Soluble Fluorescent Probe with Dual Mitochondria/Lysosome Targetability for Selective Superoxide Detection in Live Cells and in Zebrafish Embryos, ACS Sensors, 3 (2018) 59-64.

[5] W. Zhang, Y. Liu, Q. Gao, C. Liu, B. Song, R. Zhang, J. Yuan, A ruthenium(ii) complex–cyanine energy transfer scaffold based luminescence probe for ratiometric detection and imaging of mitochondrial peroxynitrite, Chemical Communications, 54 (2018) 13698-13701.

[6] R. Zhang, Z. Ye, G. Wang, W. Zhang, J. Yuan, Development of a Ruthenium(II) Complex Based Luminescent Probe for Imaging Nitric Oxide Production in Living Cells, Chemistry – A European Journal, 16 (2010) 6884-6891.

[7] B.C. Dickinson, C. Huynh, C.J. Chang, A Palette of Fluorescent Probes with Varying Emission Colors for Imaging Hydrogen Peroxide Signaling in Living Cells, Journal of the American Chemical Society, 132 (2010) 5906-5915.

[8] M.D. Hammers, M.J. Taormina, M.M. Cerda, L.A. Montoya, D.T. Seidenkranz, R. Parthasarathy, M.D. Pluth, A Bright Fluorescent Probe for H2S Enables Analyte-Responsive, 3D Imaging in Live

Zebrafish Using Light Sheet Fluorescence Microscopy, Journal of the American Chemical Society, 137 (2015) 10216-10223.

[9] Z. Du, B. Song, W. Zhang, C. Duan, Y.-L. Wang, C. Liu, R. Zhang, J. Yuan, Quantitative Monitoring and Visualization of Hydrogen Sulfide In Vivo Using a Luminescent Probe Based on a Ruthenium(II) Complex, Angewandte Chemie International Edition, 57 (2018) 3999-4004.

[10] W. Zhang, J. Kang, P. Li, H. Wang, B. Tang, Dual Signaling Molecule Sensor for Rapid Detection of Hydrogen Sulfide Based on Modified Tetraphenylethylene, Analytical Chemistry, 87 (2015) 8964-8969.

[11] C. Zhang, L. Wei, C. Wei, J. Zhang, R. Wang, Z. Xi, L. Yi, A FRET–ICT dual-quenching fluorescent probe with large off–on response for H2S: synthesis, spectra and bioimaging, Chemical Communications, 51 (2015) 7505-7508.

[12] L. Yang, Y. Su, Y. Geng, Y. Zhang, X. Ren, L. He, X. Song, A Triple-Emission Fluorescent Probe for Discriminatory Detection of Cysteine/Homocysteine, Glutathione/Hydrogen Sulfide, and Thiophenol in Living Cells, ACS Sensors, 3 (2018) 1863-1869.

[13] S.-J. Li, Y.-F. Li, H.-W. Liu, D.-Y. Zhou, W.-L. Jiang, J. Ou-Yang, C.-Y. Li, A Dual-Response Fluorescent Probe for the Detection of Viscosity and H2S and Its Application in Studying Their Cross-Talk Influence in Mitochondria, Analytical Chemistry, 90 (2018) 9418-9425.

[14] C. Wei , R. Wang , L. Wei , L. Cheng , Z. Li, Z. Xi , L. Yi o-Fluorination of Aromatic Azides Yields Improved Azido-Based Fluorescent Probes for Hydrogen Sulfide: Synthesis, Spectra, and Bioimaging, Chemistry – An Asian Journal, 9 (2014) 3586-3592.

[15] D.-T. Shi, D. Zhou, Y. Zang, J. Li, G.-R. Chen, T.D. James, X.-P. He, H. Tian, Selective fluorogenic imaging of hepatocellular H2S by a galactosyl azidonaphthalimide probe, Chemical Communications, 51 (2015) 3653-3655.

[16] S. Yang, Y. Qi, C. Liu, Y. Wang, Y. Zhao, L. Wang, J. Li, W. Tan, R. Yang, Design of a Simultaneous Target and Location-Activatable Fluorescent Probe for Visualizing Hydrogen Sulfide in Lysosomes, Analytical Chemistry, 86 (2014) 7508-7515.

[17] S. Singha, D. Kim, H. Moon, T. Wang, K.H. Kim, Y.H. Shin, J. Jung, E. Seo, S.-J. Lee, K.H. Ahn, Toward a Selective, Sensitive, Fast-Responsive, and Biocompatible Two-Photon Probe for Hydrogen Sulfide in Live Cells, Analytical Chemistry, 87 (2015) 1188-1195.

[18] N. Gupta, S.I. Reja, V. Bhalla, M. Gupta, G. Kaur, M. Kumar, A bodipy based dual functional probe for the detection of hydrogen sulfide and H2S induced apoptosis in cellular systems, Chemical Communications, 51 (2015) 10875-10878.

[19] N. Adarsh, M.S. Krishnan, D. Ramaiah, Sensitive Naked Eye Detection of Hydrogen Sulfide and Nitric Oxide by Aza-BODIPY Dyes in Aqueous Medium, Analytical Chemistry, 86 (2014) 9335-9342.

[20] Y. Yan, H. Yu, Y. Zhang, K. Zhang, H. Zhu, T. Yu, H. Jiang, S. Wang, Molecularly Engineered Quantum Dots for Visualization of Hydrogen Sulfide, ACS Applied Materials & Interfaces, 7 (2015) 3547-3553.